Ca^{2+} influx is an essential component of the positive-feedback loop that maintains leading-edge structure and activity in macrophages

John H. Evans*† and Joseph J. Falke*†‡

*Department of Chemistry and Biochemistry and the ‡Molecular Biophysics Program, University of Colorado, Boulder, CO 80309-0215

Communicated by J. Richard McIntosh, University of Colorado, Boulder, CO, August 15, 2007 (received for review December 19, 2006)

In migrating eukaryotic cells, phosphatidylinositol 3-kinase (PI3K), filamentous actin (F-actin), and monomeric Rho GTPases are key components of a complex positive-feedback system that maintains and amplifies a phosphatidylinositol-3,4,5-trisphosphate signal at the leading edge of the cell. This lipid signal is required for cell polarization and movement. In leukocytes and *Dictyostelium*, activation or inhibition of any one of these components leads to the activation or inhibition, respectively, of the others via undefined feedback interactions. The role of Ca^{2+} signals in migrating leukocytes is controversial, and there has been no indication that Ca^{2+} participates in positive feedback. Here, we demonstrate that an extracellular Ca^{2+} influx is required for positive feedback at the leading edge of spontaneously polarized macrophages. Inhibition of extracellular Ca^{2+} influx leads to loss of leading-edge PI3K activity, disassembly of F-actin, cessation of ruffling, and decay of chemoattractant signals. Conversely, increasing cytosolic Ca^{2+} enhances membrane ruffling, PI3K activity, and F-actin accumulation. Overall, these findings demonstrate that an extracellular Ca^{2+} influx is an essential component, together with PI3K and F-actin, of the positive-feedback cycle that maintains leading-edge structure and ruffling activity and that supports the chemoattractant response. Strikingly, the Ca^{2+}-sensitive enzyme protein kinase Cα (PKCα) is enriched at the leading edge, and its enrichment is sensitive to blockade of Ca^{2+} influx, to inhibition of PI3K activity, and to F-actin depolymerization. These findings support the working hypothesis that a local, leading-edge Ca^{2+} signal recruits PKCα as a central player in the positive-feedback loop.

actin | calcium | chemotaxis | phosphoinositide 3-kinase | phosphatidylinositol-3,4,5-trisphosphate

The importance of Ca^{2+} in directed cell migration has been long recognized (1–5) and controversial (6, 7). Leukocyte migration, for example, slows and stops when the Ca^{2+} is depleted from the extracellular medium or is chelated from the medium with EGTA or when the Ca^{2+} channel blocker La^{3+} is added to the extracellular medium (1–5, 8). Similarly, migration slows when the intracellular Ca^{2+} is buffered (9, 10). Furthermore, in many leukocytes, addition of exogenous phosphatidylinositol-3,4,5-trisphosphate ($PI(3,4,5)P_3$), the lipid product of PI3K, stimulates a Ca^{2+} influx, whereas PI3K inhibition blocks Ca^{2+} influx, implicating a link between PI3K and Ca^{2+} signaling (11–13). All of these observations suggest that Ca^{2+} plays an important, but undefined, role in cell polarization or migration. However, the function of Ca^{2+} in leukocyte migration has not yet been determined, and current models for leading-edge maintenance and signaling do not propose a role for Ca^{2+} (14–16).

The formation of an actively ruffling leading edge is a key cellular event that always precedes migration, and maintenance of a leading edge is required for persistent migration (14–16). The present study investigates the potential link between Ca^{2+} signaling and leading-edge maintenance by fluorescence imaging in live RAW264.7 mouse macrophages (hereafter referred to as RAW cells). Using fluorescent proteins to determine the cellular localizations of PI3K activity, actin, and PKCα, the study finds that an extracellular Ca^{2+} influx (*i*) participates in a positive-feedback cycle with PI3K and F-actin activities at the leading edge, (*ii*) contributes to the organization and maintenance of an actively ruffling leading edge, (*iii*) localizes PKCα to the ruffling leading edge, and (*iv*) supports prolonged stimulation of PI3K activity by chemoattractant.

Results

Characterization of Polarized RAW Cells as a Model System for the Macrophage Leading Edge. To investigate the contribution of Ca^{2+} signaling to leading-edge structure and function, we used spontaneously polarized RAW cells as a macrophage model system. We have found that RAW cells display spontaneous polarization when plated on glass and exhibit active ruffling of the leading-edge membrane [Fig. 1*A* and supporting information (SI) Movie 1]. Because the trailing end of these cells adheres tightly to the glass, the cell becomes quite elongated and fails to crawl, yielding a spatially and kinetically stable leading edge. The resulting polarized cell is an ideal model system for quantitating the cellular processes essential for leading-edge maintenance and signaling.

The establishment of cell polarity required for spontaneous and chemotactic cell movement is believed to involve a positive-feedback loop that self-organizes the leading edge of migrating amoeboid cells ranging from *Dictyostelium* to leukocytes (15–19). The currently identified components of this feedback system are (*i*) activation of PI3K to produce the signaling lipids $PI(3,4,5)P_3$ and $PI(3,4)P_2$ (18, 20), (*ii*) polymerization of actin (19, 21), and (*iii*) activation of the monomeric GTPase Rac1 (22, 23). To assay for PI3K activity, we used GFP fused to the Akt1 pleckstrin homology (PH) domain (GFP-Akt1PH), which binds specifically to $PI(3,4,5)P_3$ and $PI(3,4)P_2$ and is widely used as a PI3K activity sensor (24). GFP-Akt1PH was observed to accumulate at the leading edge of ruffling RAW cells (Fig. 1 *B–D* and SI Fig. 5*A*), and its accumulation was stable for long periods (>15 min) (SI Fig. 5*B* and SI Movie 2). To visualize F-actin, we used both (*i*) GFP fused to β-actin (GFP-actin), which incorporates into F-actin filaments, and (*ii*) fluorescently labeled phalloidin, which preferentially stains F-actin. Both probes were found predominantly in leading-edge ruffles (Fig. 1 *B–D* and SI Fig. 5*A*). Finally, to observe Rac1, we stained cells with fluorescent anti-Rac1 antibody, which also localized predominantly to the leading edge (SI Fig. 5*A*). Thus, all three components of the established positive-feedback loop targeted preferentially to

Author contributions: J.H.E. designed research; J.H.E. performed research; J.H.E. analyzed data; and J.H.E. and J.J.F. wrote the paper.

The authors declare no conflict of interest.

Abbreviation: RAW cells, RAW264.7 mouse macrophages.

†To whom correspondence may be addressed. E-mail: john.evans@colorado.edu or joseph.falke@colorado.edu.

This article contains supporting information online at www.pnas.org/cgi/content/full/0707719104/DC1.

© 2007 by The National Academy of Sciences of the USA

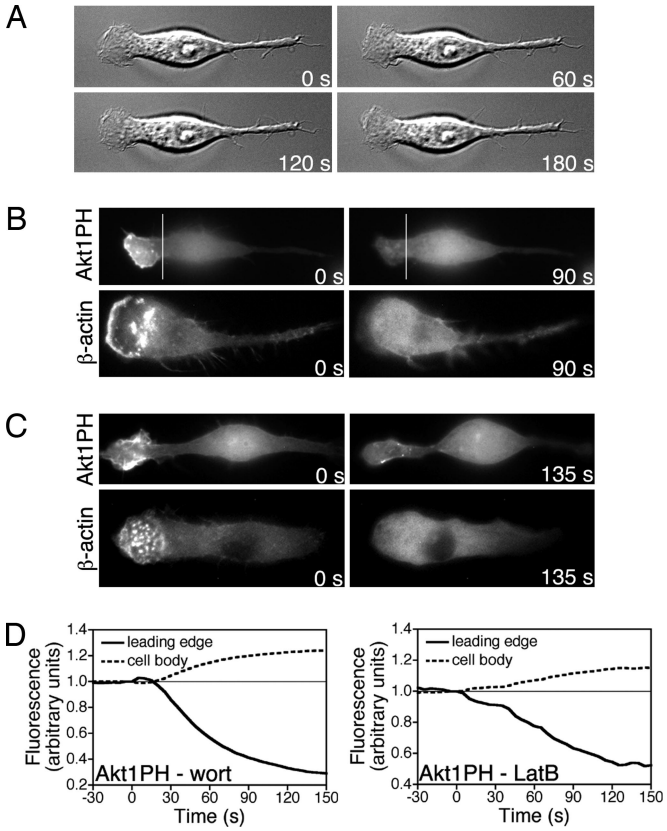

Fig. 1. Characterization of polarized RAW cells. (*A*) Wild-type, polarized RAW cells imaged at 5-s intervals as visualized by Nomarski optics, illustrating the pronounced, ruffling leading edge. (*B* and *C*) Time-lapse fluorescence images of spontaneously polarized RAW cells expressing GFP-Akt1PH (*Upper*) or GFP-actin (*Lower*) treated with 500 nM wortmannin (WORT) (*B*) or 10 μg ml^{-1} latrunculin B (LatB) (*C*). Images show the cell at the time indicated relative to drug addition, illustrating the redistribution of fluorescent protein from the leading-edge region to the cell body (defined as the regions to the left and right of the vertical bar, respectively) after treatment. For each time series, the intensity scaling was the same for all images. Images are representative of at least five experiments. (*D*) Plots show the integrated GFP-Akt1PH fluorescence versus time for the leading-edge and cell body regions before and after wortmannin (*Left*) or LatB (*Right*) addition, thereby quantitating the transfer of fluorescent protein from the leading edge to the cell body after treatment. See also SI Movies 1, 3, and 5–7 for *A*, *B*, and *C*.

the leading-edge membrane and ruffles of polarized cells. These enrichments of Akt1, F-actin, and Rac1 at the leading edge arose from specific recruitment of these components and not simply from increased membrane density or cytoplasmic volume in the ruffling region (see multiple controls in SI Fig. 5 *A–E*).

To directly test whether spontaneously polarized RAW cells possess a PI3K/F-actin positive-feedback loop at their leading edge, we next investigated the consequence of inhibiting PI3K activity or F-actin treadmilling in ruffling cells expressing GFP-Akt1PH or GFP-actin. The PI3K inhibitor wortmannin decreases PI(3,4,5)P_3 at the leading edge of cells by inhibiting its production, whereas phosphatases continue to hydrolyze it (25). Wortmannin treatment of cells caused rapid loss of GFP-Akt1PH from the leading edge and stopped ruffling (Fig. 1*B Upper* and SI Movie 3). Quantitative analysis of GFP-Akt1PH fluorescence shows that, upon wortmannin treatment, the leading-edge region experiences a large loss of fluorescence on the same time scale as a significant fluorescence increase is observed in the cell body (Fig. 1*D*, left plot and SI Fig. 6*A*). DMSO, the vehicle for wortmannin, affected neither ruffling nor the cellular distribution of GFP-Akt1PH (SI Fig. 6*B* and SI Movie 4). Treatment with wortmannin also caused loss of GFP-actin from the leading-edge ruffles (Fig. 1*B Lower* and SI Movie 5), as predicted by the positive-feedback hypothesis requiring an essential link between PI3K activity and F-actin polymerization.

Latrunculin B (LatB) sequesters monomeric actin and prevents F-actin polymerization, resulting in loss of lamellipodial structure (18). In polarized cells, GFP-actin at the leading edge was rapidly lost after LatB treatment (Fig. 1*C Lower* and SI Movie 6). Consistent with the positive-feedback hypothesis, LatB treatment also caused loss of GFP-Akt1PH from the leading edge (Fig. 1*C Upper*; Fig. 1*D*, right plot; and SI Movie 7). Interestingly, the mechanism of Akt1PH loss from the leading-edge membrane during LatB treatment appears qualitatively different from its loss in response to wortmannin (compare Fig. 1 *B Upper* and *C Upper*). In addition to simple dissociation from membrane, internalization of Akt1PH-bound plasma membrane is also observed (best seen in SI Movie 7). In sum, these observations demonstrate that a positive-feedback loop involving PI3K and F-actin regulates leading-edge ruffling in RAW cells, as in other leukocytes.

A Ca^{2+} Influx Maintains PI3K Activity, F-Actin Polymerization, and Ruffling in RAW Cells. Because leukocyte migration both requires a functional positive-feedback loop at the leading edge (18, 26, 27) and is inhibited by blocking Ca^{2+} influx (1–5, 8), we next investigated whether blockade of Ca^{2+} influx disrupts the PI3K/F-actin positive-feedback loop. To test this possibility, we examined the effects of reagents that block extracellular Ca^{2+} influx [EGTA, La^{3+}, and the organic Ca^{2+} channel inhibitor SKF 96365 (SKF)] on the distribution of GFP-Akt1PH and GFP-actin in polarized cells. We found that all three agents produced a loss of GFP-Akt1PH from the leading edge within 2–3 min, concomitant with a loss of membrane ruffling (Fig. 2*A* and SI Movies 8–10). Addition of imaging buffer (vehicle for EGTA and La^{3+}) or DMSO (vehicle for SKF) had no effect on ruffling or on the distribution of GFP-Akt1PH (SI Fig. 6 *B* and *C*). Quantitation of GFP-Akt1PH fluorescence demonstrates that the intensity loss from the leading edge is simultaneous with the intensity increase in the cell body, indicating a dramatic loss of PI(3,4,5)P_3/PI(3,4)P_2 at the leading edge. In parallel experiments, we found no redistribution of fluorescence of the PI(4,5)P_2 sensor GFP-PLCδ_1PH in response to SKF, wortmannin, or LatB (SI Fig. 7*A*), suggesting that these agents affect the distribution of PI(3,4,5)P_3/PI(3,4)P_2 but not PI(4,5)P_2. It follows that an extracellular Ca^{2+} influx is required for sustained PI3K activity during maintenance of an active leading edge.

Similarly, we found that EGTA, La^{3+}, and SKF addition caused rapid loss of leading-edge GFP-actin within 2 min of addition (Fig. 2*B* and SI Movie 11). Nomarski imaging of wild-type cells similarly showed a collapse of the leading edge and ruffles in response to EGTA or SKF treatment (Fig. 2*C* and SI Fig. 8, respectively, and SI Movies 12 and 13). Together, our results strongly suggest that Ca^{2+} influx participates in the established PI3K/F-actin positive-feedback loop, because both PI3K activity and F-actin-associated ruffling require influx of extracellular Ca^{2+}.

Our hypothesis that Ca^{2+} influx is a required component of the positive-feedback loop predicts that a cytoplasmic Ca^{2+} increase will stimulate PI3K activity and F-actin turnover, yielding enhanced ruffling. To test this prediction, we next stimulated polarized, ruffling cells with ATP, which elicits global cytoplasmic Ca^{2+} signals in macrophages (28) and many other cell types (29). Ruffling cells expressing GFP-Akt1PH and, stimulated with ATP, exhibited a large, transient increase in GFP-Akt1PH fluorescence at the leading edge (SI Fig. 9*A* and SI Movie 14). In addition, large local increases were observed at ectopic ruffles

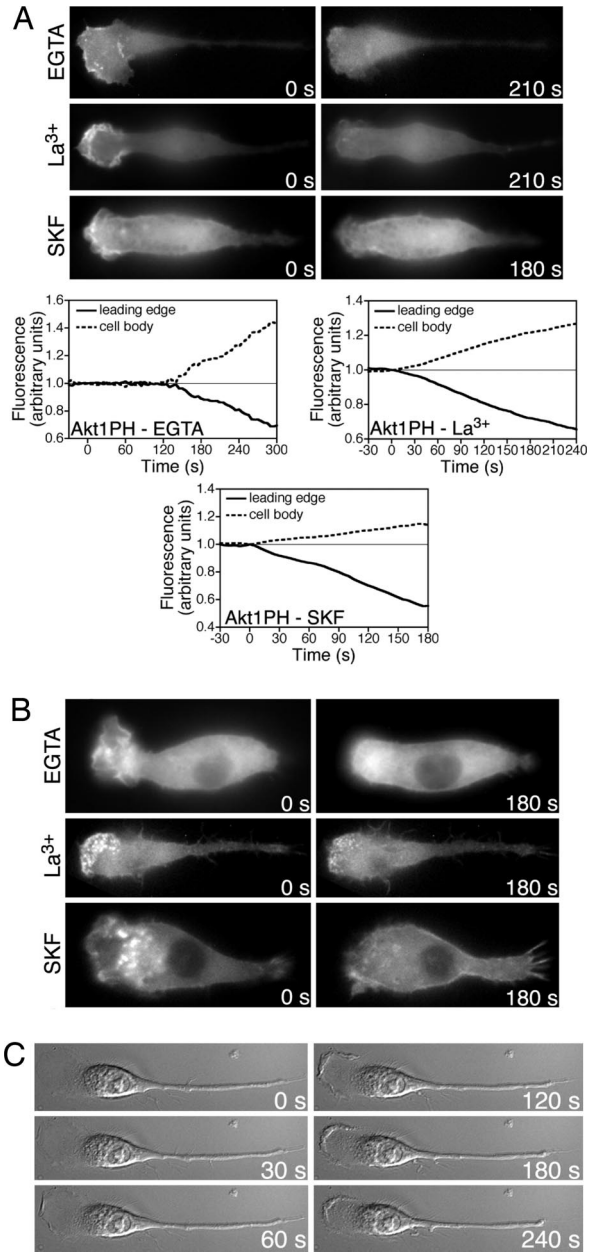

Fig. 2. Inhibition of extracellular Ca^{2+} influx results in loss of PI3K activity, F-actin, and ruffling from the leading edge. (*A* and *B*) Time-lapse fluorescence images of RAW cells expressing GFP-Akt1PH (*A*) or GFP-actin (*B*) treated with 3 mM EGTA (*Top*), 1 mM $LaCl_3$ (*Middle*), or 20 μM SKF (*Bottom*). Indicated times are relative to drug addition. The images show the transfer of fluorescent protein from the leading-edge region to the cell body after drug addition, as do the accompanying plots of integrated GFP-Akt1PH fluorescence. (*C*) Nomarski images of wild-type cell treated with 3 mM EGTA at the indicated time, illustrating the loss of ruffling and retraction of the leading edge after treatment. For each time series, the intensity scaling was the same for all images. Images are representative of at least five experiments. See also SI Movies 8–12 for *A*, *B*, and *C*.

outside the leading edge and at the tip of the uropod, and a small, transient fluorescence increase was observed along the plasma membrane of the cell body (SI Fig. 9*A* and SI Movie 14). The latter findings suggest that the positive-feedback loop is operating in all regions of the plasma membrane but is normally suppressed by lipid phosphatases and that such suppression can be overridden by a large Ca^{2+} signal. As expected from the observed increase in ruffling, ATP also transiently increased GFP-actin at the leading edge, at the ectopic ruffle sites, and at the tip of the uropod (SI Fig. 10*A* and SI Movie 15). In contrast, ATP caused no fluorescence increase for the $PI(4,5)P_2$ sensor GFP-PLCδ_1PH at the leading edge, ectopic ruffles, or the uropod (SI Fig. 7*B*), suggesting that ATP specifically increases the $PI(3,4,5)P_3/PI(3,4)P_2$ products of PI3K activity at these locations but not $PI(4,5)P_2$.

We also examined the effects of ATP on nonruffling RAW cells presumed to have no preexisting, active positive-feedback loop. In these cells, global addition of ATP caused no change in the intracellular distribution of GFP-Akt1PH or GFP-actin (SI Figs. 9*B* and 10*B*, respectively) in contrast to global addition of chemotactic peptide C5a (24), which directly stimulated PI3K and elicited global translocation of GFP-Akt1PH to the plasma membrane in both ruffling and nonruffling cells (SI Fig. 9 *C* and *D* and SI Movie 16). Together, these results indicate that polarized cells possess an active positive-feedback loop driving a ruffling leading edge and that feedback-loop activity can be amplified by additional release of a Ca^{2+} into the cytoplasm, confirming our hypothesis that Ca^{2+} is an essential component of positive feedback at the leading edge.

Localized PKCα Recruitment at the Leading Edge Requires Ca^{2+} Influx, PI3K Activity, and F-Actin. Plasma membrane targeting of PKCα to the plasma membranes of mammalian cells is driven by the binding of Ca^{2+}, $PI(4,5)P_2$, and phosphatidylserine to its C2 domain (30, 31). Once the C2 domain is docked to the membrane, diacylglycerol (DAG) can bind to the PKCα C1 domain (32–35). Because $PI(4,5)P_2$ is distributed homogeneously throughout the inner plasma membrane leaflet of polarized RAW cells (SI Fig. 5*C Lower* and SI Movie 17), and because DAG binding can occur only when the protein is already docked to the membrane during a Ca^{2+} signal (32–35), a Ca^{2+} signal alone is necessary and sufficient to trigger recruitment of YFP-PKCα to plasma membrane, making PKCα useful as a Ca^{2+} sensor (36). Thus, addition of ATP, which elicits a global and transient Ca^{2+} signal, produced a global and transient recruitment of YFP-PKCα to plasma membrane in both ruffling and nonruffling cells (Fig. 3*C* and SI Fig. 11, respectively, and SI Movie 18).

Strikingly, in unstimulated, ruffling cells, the YFP-PKCα Ca^{2+} sensor is stably enriched at the ruffling leading edge (Fig. 3 *A–C* and SI Fig. 5*C Middle*). This finding suggests that a local cytoplasmic Ca^{2+} signal similar to that reported at the leading edge of chemotaxing primary neutrophils (9) may exist in polarized RAW cells. Upon addition of a Ca^{2+} influx blocker, either EGTA or La^{3+}, a rapid loss of YFP-PKCα was observed from the leading edge, and membrane ruffling ceased (Fig. 3*A Upper* and *Lower*, respectively, and SI Movies 19 and 20). Quantitative analysis of the fluorescence distribution clearly demonstrated that the blockade of Ca^{2+} influx caused a dramatic redistribution of YFP-PKCα from the leading edge to the cell body. Similarly, wortmannin and LatB also triggered rapid loss of YFP-PKCα from the leading edge of polarized, ruffling cells (Fig. 3*B* and SI Movies 21 and 22), although the response to LatB is qualitatively different from the response to wortmannin as noted above (Fig. 1 *B* and *C*). These results indicate that an influx of extracellular Ca^{2+} is essential for a local, leading-edge Ca^{2+} signal detected in the cytoplasm by YFP-PKCα and that this local Ca^{2+} signal can be inhibited either by blocking Ca^{2+} influx or by disruption of the positive-feedback loop.

A Ca^{2+} Influx Maintains PI3K Activity in Chemoattractant-Stimulated RAW Cells. To ascertain whether the extracellular Ca^{2+} influx is essential for chemoattractant signaling, we next tested the effect of blocking Ca^{2+} influx on PI3K activity in RAW cells stimulated with chemoattractant lipopolysaccharide (LPS). RAW cells

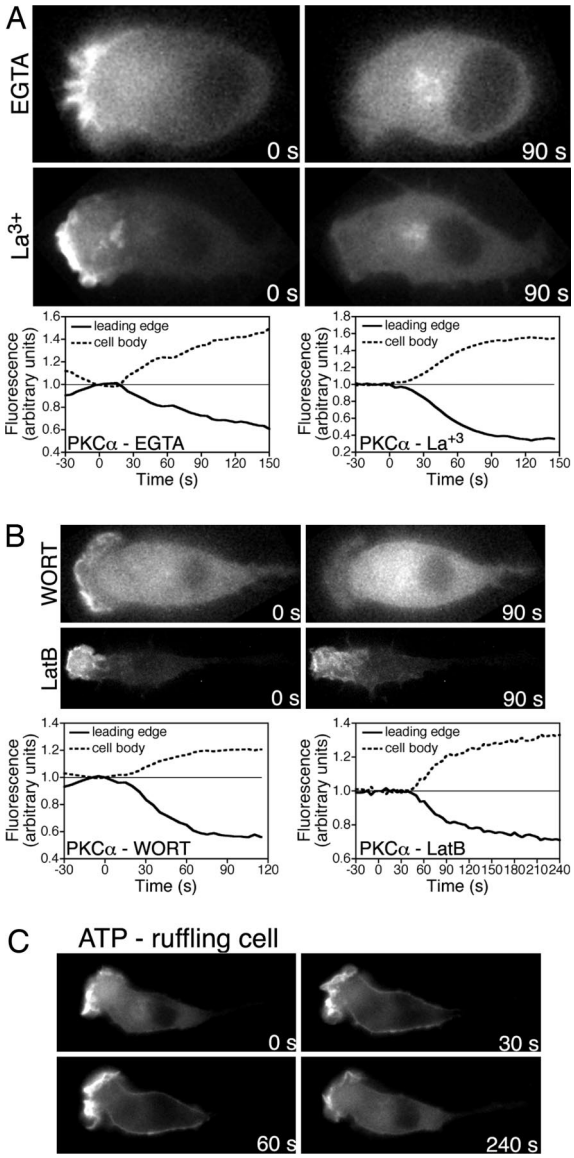

Fig. 3. Recruitment of PKCα to the leading edge is sensitive to extracellular Ca^{2+} influx, PI3K activity, and F-actin polymerization. (*A*) Time-lapse fluorescence images of polarized RAW cells expressing YFP-PKCα treated with 3 mM EGTA (*Upper*) or 1 mM $LaCl_3$ (*Lower*). Plots show the integrated YFP-PKCα fluorescence versus time for the leading-edge and cell body regions before and after drug addition. Both the images and plots reveal a significant transfer of YFP-PKCα from the leading edge to the cell body after blockade of Ca^{2+} influx. (*B*) Time-lapse fluorescence images of polarized RAW cells expressing YFP-PKCα treated with 500 nM wortmannin (WORT) (*Upper*) or 10 μg ml^{-1} latrunculin B (LatB) (*Lower*). Plots show the integrated YFP-PKCα fluorescence versus time for the leading-edge and cell-body regions before and after drug addition. Both the images and plots illustrate the redistribution of YFP-PKCα from the leading edge to the cell body after treatment. (*C*) Time-lapse fluorescence images of a ruffling RAW cells expressing YFP-PKCα treated with global addition of 25 μM ATP, showing a large increase in fluorescence at the leading-edge plasma membrane as well as a global targeting to plasma membrane throughout the cell body. Indicated times are relative to addition of drug. For each time series, the intensity scaling was the same for all images. Images are representative of at least five experiments. See also SI Movies 18–22 for *A*, *B*, and *C*. Both wortmannin and LatB cause dissociation of YFP-PKCα from the leading edge; in addition, LatB causes loss of YFP-PKCα through internalization of plasma membrane, as best seen in SI Movie 21.

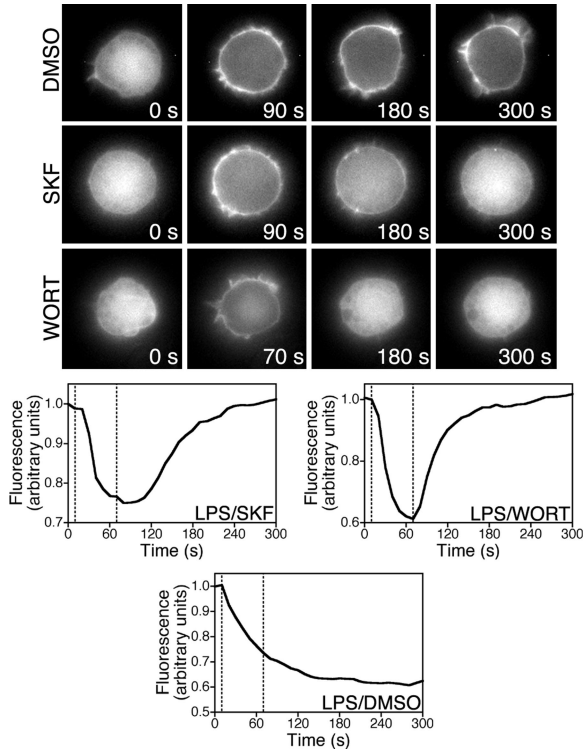

Fig. 4. Inhibition of extracellular Ca^{2+} influx or PI3K reverses the accumulation of $PI(3,4,5)P_3$ at the plasma membrane in LPS-treated cells. Time-lapse fluorescence images of nonpolarized RAW cells plated on fibronectin and expressing GFP-Akt1PH. Shown are cells before and after treatment with 10 μM LPS at 10 s, followed by treatment at 70 s with 0.1% DMSO (*Top*), 20 μM SKF (*Middle*), or 500 nM wortmannin (*Bottom*). Plots show average pixel intensity of Akt1PH fluorescence in the cytosol before and after drug additions. Indicated times are relative to drug addition. Both images and plots indicate that the carrier (DMSO) has no effect, whereas the Ca^{2+} channel blocker (SKF) and PI3K inhibitor [wortmannin (WORT)] both inhibit the PI3K activity in attractant-stimulated cells. For each time series, the intensity scaling was the same for all images. Vertical dotted lines indicate addition of LPS (*Left*) and either SKF, wortmannin, or DMSO (*Right*). Images are representative of at least three experiments. See also SI Movie 23.

plated on a dense fibronectin substrate exhibited no polarization, PI3K activity, or ruffling and, thus, lacked a detectable positive-feedback loop. Nonpolarized cells expressing GFP-Akt1PH and stimulated with LPS exhibited a striking global translocation of GFP-Akt1PH to the plasma membrane as the result of LPS-generated PI3K activity, which persisted for several minutes and was accompanied by membrane outgrowth (Fig. 4*A Top* and SI Movie 23). However, addition of the extracellular Ca^{2+} influx blocker SKF 70 seconds after stimulation with LPS dramatically shortened the PI3K response to LPS (Fig. 4*A Middle*) in a fashion similar to the addition of the PI3K antagonist wortmannin (Fig. 4*A Bottom*). Fluorescence analysis confirmed the reversal of GFP-Akt1PH translocation, from the plasma membrane back to the cytosol, in response to both SKF and wortmannin treatment. Treatment of LPS-stimulated cells with LatB also displaced GFP-Akt1PH from the plasma membrane as well as triggering membrane internalization as previously seen in other chemoattractant-stimulated leukocytes (SI Fig. 12 and SI Movie 24) (18). Together, these findings indicate that extracellular Ca^{2+} influx plays an essential role in maintenance of PI3K activity and F-actin polymerization in cells stimulated with chemoattractant.

Discussion

Together, the above evidence reveals that an extracellular Ca^{2+} influx is essential for the organization and maintenance of an active leading edge in RAW macrophages. Inhibitors of the Ca^{2+} influx

CELL BIOLOGY

cause the leading edge to collapse and disrupt both PI3K activity and F-actin, whereas an increase in cytoplasmic Ca^{2+} stimulates ruffling and enhances PI3K and F-actin. Moreover, inhibition of either PI3K activity or F-actin polymerization blocks the Ca^{2+} signal while disrupting the leading edge. As a result, the Ca^{2+} signal must now be considered a necessary component, along with PI3K and F-actin activity, of the positive-feedback loop that underlies leading-edge stability and activity. Although the spontaneously polarized RAW cells used in the present study were not chemotaxing, previous studies of chemotaxing neutrophils have shown that blockade of Ca^{2+} entry with extracellular EGTA or La^{3+} blunts Ca^{2+} signaling and directed cell migration (1–5), and the present study shows that Ca^{2+} influx in RAW cells is necessary for prolonged PI3K activity in response to chemoattractant. It follows that Ca^{2+} influx and the positive-feedback loop in which it participates are likely to play central roles in leukocyte polarization, leading-edge maintenance, and chemoattractant signaling.

We also present evidence that PKCα is specifically recruited to the leading edge of spontaneously polarized, actively ruffling RAW cells. The simplest explanation for this observation is that the essential Ca^{2+} influx involved in the positive-feedback loop triggers or maintains a localized, cytoplasmic Ca^{2+} signal at the leading edge. It is not yet clear whether this Ca^{2+} signal arises predominantly from the extracellular Ca^{2+} influx or, rather, from intracellular Ca^{2+} stores. In the latter case, the extracellular Ca^{2+} influx would be required to trigger release from intracellular stores, or replenish intracellular stores. In either case, the resulting localized Ca^{2+} signal activates the PKCα C2 domain, which recruits the protein to the plasma membrane. In an attempt to image Ca^{2+} at the leading edge, we loaded minimal quantities of the fluorescent Ca^{2+} indicators Fluo3-AM and FuraRed-AM into ruffling RAW cells. However, these small-molecule Ca^{2+} indicators eliminated ruffling and localization of the PI3K activity sensor GFP-Akt1PH at the leading edge (data not shown). Such leading-edge collapse presumably arose from the well documented Ca^{2+} buffering effects of these highly mobile, high-affinity Ca^{2+} chelators (37, 38), which would buffer low magnitude Ca^{2+} signals. Overall, the small-molecule Ca^{2+} indicator studies failed to provide additional information on the spatial extent of the Ca^{2+} signal, but they did provide further evidence highlighting the importance of Ca^{2+} signaling in leading-edge structure and activity.

The identity of the plasma membrane Ca^{2+} channel responsible for the required Ca^{2+} influx is unknown, but two plausible candidates exist. One is a subfamily of noncapacitative, $PI(3,4,5)P_3$-gated Ca^{2+} influx channels of the transient receptor potential (TRP) class (39). Such TRP channels have been described in leukocytes (11, 12, 40) and in neuronal growth cones (41, 42). The other is a Ca^{2+} channel regulated by extracellular ATP, which could either directly gate the channel or activate a signaling pathway leading to channel gating. Recent evidence indicates that local secretion of ATP at the leading edge of chemotaxing neutrophils is essential for gradient sensing (43), which raises the possibility of a link between ATP secretion and Ca^{2+} influx.

Finally, several possibilities exist for the circuit connections between the leading-edge Ca^{2+} signal and the PI3K/F-actin positive-feedback loop. In other cells, Rac1 has been implicated in the PI3K/F-actin positive-feedback loop (17, 22), but we have not yet directly assessed the role of Rac1 activity in the RAW macrophage Ca^{2+}/PI3K/F-actin feedback loop. Given that Rac1 may also participate, one intriguing possibility is the involvement of CAPRI, a Rac1 scaffold protein containing two C2 domains that promote Ca^{2+}-dependent membrane translocation (44). CAPRI has been shown to be necessary for Rac1 translocation to macrophage phagosomes (45), which also exhibit a local Ca^{2+} signal during phagocytosis (9). Thus, a Ca^{2+}/CAPRI-dependent mechanism for Rac1 targeting could serve to augment signaling from Rac1-sensitive PI3Kγ (46). An equally intriguing possibility is that the Ca^{2+}-triggered recruitment of endogenous PKCα, which we have observed in the polarized RAW macrophages (data not shown), could be required for phosphorylation of MARCKS (47, 48), which is linked to $PI(4,5)P_2$ sequestration and actin remodeling.

In closing, excessive macrophage migration plays an important role in inflammatory diseases such as asthma (49), chronic obstructive pulmonary disease (50), and rheumatoid arthritis (51). Thus, targeting the channels or effectors responsible for the essential Ca^{2+} influx could represent a strategy in developing therapeutics for these diseases. More broadly, further studies are needed to determine the generality of the Ca^{2+} influx in other migrating cells and to elucidate its fundamental molecular mechanisms.

Materials and Methods

Materials. RAW264.7 murine macrophage-like cells were obtained from the American Type Culture Collection (Manassas, VA). Antibiotic G418, latrunculin B, LPS, wortmannin, SKF96365, ATP, fibronectin, and endotoxin-free BSA were from Sigma (St. Louis, MO). TRITC-conjugated anti-Rac1 was from BD Transduction Laboratories (Lexington, KY). Alexa Fluor 488-phalloidin and Lipofectamine 2000 were from Invitrogen (Carlsbad, CA). pEGFP-Akt1PH was subcloned from IMAGE clone 4562823 (residues 1–120) into pEGFP(C1) (Invitrogen). Construction of pYFP-PKCα and pGFP-PLCδ_1PH was described (30). EGFP-actin was a gift from N. Ahn (University of Colorado).

Cell Culture. Cells were cultured and transfected as described (31), and stable cell lines were produced by using antibiotic G418. Before experiments, stably transfected cells were cultured on glass-bottomed 35-mm dishes (MatTek, Ashland, MA) in culture medium without antibiotics at 1×10^5 cells per plate for a minimum of 3–4 h to allow cells to establish a polarized morphology. For experiments in Fig. 4 and SI Fig. 12, cells were plated on dishes treated with human fibronectin.

Live-Cell Fluorescent Protein Imaging. Live-cell imaging experiments were performed as described (31). Final images were produced by using Adobe Photoshop (Adobe Systems, Mountain View, CA) and ImageJ (National Institutes of Health, Bethesda, MD; http://rsb.info.nih.gov/ij/). Videos were produced with ImageJ and QuickTime Pro.

Image Analysis. Analysis of fluorescence distribution in cells in Figs. 1, 2, and 4 was performed by integrating the background- and bleach-corrected fluorescence from the leading-edge region (defined by ruffles) and cell body (see diagram in SI Fig. 6*A*). Fluorescence change with respect to time was normalized to the fluorescence values of the leading-edge region and cell body at $t = 0$ s. Analysis of fluorescence distribution in Fig. 4 was performed by determining the background- and bleach-corrected average pixel intensity from the cytosolic region of the cells.

This work was supported by National Institutes of Health Grant R01 GM063235 (to J.J.F.).

1. Becker EL, Showell HJ (1972) *Z Immunitatsforsch Exp Klin Immunol* 143:466–476.
2. Gallin JI, Rosenthal AS (1974) *J Cell Biol* 62:594–609.
3. Wilkinson PC (1975) *Exp Cell Res* 93:420–426.
4. Estensen RD, Reusch ME, Epstein ML, Hill HR (1976) *Infect Immun* 13:146–151.
5. Boucek MM, Snyderman R (1976) *Science* 193:905–907.
6. Zigmond SH (1977) *J Cell Biol* 75:606–616.
7. Marasco WA, Becker EL, Oliver JM (1980) *Am J Pathol* 98:749–768.
8. Mandeville JT, Ghosh RN, Maxfield FR (1995) *Biophys J* 68:1207–1217.
9. Sawyer DW, Sullivan JA, Mandell GL (1985) *Science* 230:663–666.
10. Marks PW, Maxfield FR (1990) *J Cell Biol* 110:43–52.
11. Ching TT, Hsu AL, Johnson AJ, Chen CS (2001) *J Biol Chem* 276:14814–14820.

12. Hsu AL, Ching TT, Sen G, Wang DS, Bondada S, Authi KS, Chen CS (2000) *J Biol Chem* 275:16242–16250.
13. Tian W, Laffafian I, Dewitt S, Hallett MB (2003) *EMBO Rep* 4:982–988.
14. Parent CA (2004) *Curr Opin Cell Biol* 16:4–13.
15. Franca-Koh J, Kamimura Y, Devreotes P (2006) *Curr Opin Genet Dev* 16:333–338.
16. Charest PG, Firtel RA (2006) *Curr Opin Genet Dev* 16:339–347.
17. Weiner OD, Neilsen PO, Prestwich GD, Kirschner MW, Cantley LC, Bourne HR (2002) *Nat Cell Biol* 4:509–513.
18. Wang F, Herzmark P, Weiner OD, Srinivasan S, Servant G, Bourne HR (2002) *Nat Cell Biol* 4:513–518.
19. Xu J, Wang F, Van Keymeulen A, Herzmark P, Straight A, Kelly K, Takuwa Y, Sugimoto N, Mitchison T, Bourne HR (2003) *Cell* 114:201–214.
20. Funamoto S, Milan K, Meili R, Firtel RA (2001) *J Cell Biol* 153:795–810.
21. Weiner OD, Servant G, Welch MD, Mitchison TJ, Sedat JW, Bourne HR (1999) *Nat Cell Biol* 1:75–81.
22. Srinivasan S, Wang F, Glavas S, Ott A, Hofmann F, Aktories K, Kalman D, Bourne HR (2003) *J Cell Biol* 160:375–385.
23. Park KC, Rivero F, Meili R, Lee S, Apone F, Firtel RA (2004) *EMBO J* 23:4177–4189.
24. Servant G, Weiner OD, Herzmark P, Balla T, Sedat JW, Bourne HR (2000) *Science* 287:1037–1040.
25. Funamoto S, Meili R, Lee S, Parry L, Firtel RA (2002) *Cell* 109:611–623.
26. Watanabe N, Mitchison TJ (2002) *Science* 295:1083–1086.
27. Arrieumerlou C, Meyer T (2005) *Dev Cell* 8:215–227.
28. Qiu ZH, Gijon MA, de Carvalho MS, Spencer DM, Leslie CC (1998) *J Biol Chem* 273:8203–8211.
29. Dubyak GR, el-Moatassim C (1993) *Am J Physiol* 265:C577–606.
30. Evans JH, Murray D, Leslie CC, Falke JJ (2006) *Mol Biol Cell* 17:56–66.
31. Corbin JA, Evans JH, Landgraf KE, Falke JJ (2007) *Biochemistry* 46:4322–4336.
32. Raghunath A, Ling M, Larsson C (2003) *Biochem J* 370:901–912.
33. Oancea E, Meyer T (1998) *Cell* 95:307–318.
34. Medkova M, Cho W (1999) *J Biol Chem* 274:19852–19861.
35. Lenz JC, Reusch HP, Albrecht N, Schultz G, Schaefer M (2002) *J Cell Biol* 159:291–302.
36. Reither G, Schaefer M, Lipp P (2006) *J Cell Biol* 174:521–533.
37. Neher E, Augustine GJ (1992) *J Physiol* 450:273–301.
38. Sala F, Hernandez-Cruz A (1990) *Biophys J* 57:313–324.
39. Kwon Y, Hofmann T, Montell C (2007) *Mol Cell* 25:491–503.
40. Ramsey IS, Delling M, Clapham DE (2006) *Annu Rev Physiol* 68:619–647.
41. Wang GX, Poo MM (2005) *Nature* 434:898–904.
42. Li Y, Jia YC, Cui K, Li N, Zheng ZY, Wang YZ, Yuan XB (2005) *Nature* 434:894–898.
43. Chen Y, Corriden R, Inoue Y, Yip L, Hashiguchi N, Zinkernagel A, Nizet V, Insel PA, Junger WG (2006) *Science* 314:1792–1795.
44. Lockyer PJ, Kupzig S, Cullen PJ (2001) *Curr Biol* 11:981–986.
45. Zhang J, Guo J, Dzhagalov I, He YW (2005) *Nat Immunol* 6:911–919.
46. Suire S, Hawkins P, Stephens L (2002) *Curr Biol* 12:1068–1075.
47. Hartwig JH, Thelen M, Rosen A, Janmey PA, Nairn AC, Aderem A (1992) *Nature* 356:618–622.
48. Myat MM, Anderson S, Allen LA, Aderem A (1997) *Curr Biol* 7:611–614.
49. Peters-Golden M (2004) *Am J Respir Cell Mol Biol* 31:3–7.
50. Barnes PJ (2004) *COPD* 1:59–70.
51. Kinne RW, Brauer R, Stuhlmuller B, Palombo-Kinne E, Burmester GR (2000) *Arthritis Res* 2:189–202.